Available online at www.sciencedirect.com
SCIENCE DIRECT
Journal of Solid State Chemistry 179 (2006) 1857–1863
JOURNAL OF SOLID STATE CHEMISTRY
www.elsevier.com/locate/jssc

Rapid communication

Oxidation products of the niobium tungsten oxide $Nb_4W_{13}O_{47}$: A high-resolution scanning transmission electron microscopy study

Frank Krumeich*, Reinhard Nesper

Laboratory of Inorganic Chemistry, ETH Zurich, CH-8093 Zurich, Switzerland

Received 12 December 2005; received in revised form 16 February 2006; accepted 16 February 2006
Available online 6 March 2006

Abstract

$Nb_4W_{13}O_{47}$, a member of the solid solution series $Nb_{8-n}W_{9+n}O_{47}$ ($0 \leqslant n \leqslant 5$), crystallizes in a threefold superstructure of the tetragonal tungsten bronze structure. While the oxidation of this reduced phase at $T_{OX} = 1200\,^{\circ}C$ leads to a separation into the thermodynamically stable phases, lower oxidation temperatures result in products that comprise new structural elements and ordering variants. The characterization of the oxidation products obtained at $T_{OX} = 1000\,^{\circ}C$ was performed by scanning transmission electron microscopy applying a high-angle annular dark field detector. At the selected imaging conditions (Z contrast), not only the metal positions are revealed by this technique but valuable additional information about the elemental distribution can be obtained simultaneously.

Keywords: Niobium tungsten oxide; Electron microscopy; STEM; Z contrast; Lattice image

1. Introduction

Around 1970, the development of transmission electron microscopes with a point-to-point resolution of better than 4 Å represented a unique milestone in the history of high-resolution transmission electron microscopy (HRTEM) because achieving this resolution rendered it possible to obtain lattice images of inorganic structures for the first time. The structure of $Nb_4W_7O_{31}$, an intergrowth between the ReO_3 type and the tetragonal tungsten bronze (TTB) type, in fact was one of the first inorganic crystal structures exclusively determined by means of the HRTEM method [1]. In general, such quasi-two-dimensional structures can directly be observed in projection along the short crystallographic axis since the metal positions are visible as dark spots in HRTEM images recorded close to Scherzer defocus. Today, scanning transmission electron microscopy (STEM) represents an alternative technique for the investigation of such structures. Scanning a tiny, fully focused electron beam over the crystal while simultaneously recording electrons scattered to high angles (Rutherford scattering) with a high-angle annular dark field detector (HAADF-STEM) leads to highly resolved structure images that reveal the metal positions in projection. Besides that, this method provides additional information about the elemental distribution since the intensity of an atom column in the image increases in proportion to almost the square of the atomic number (Z contrast) [2–4]. The applicability of this method has recently been demonstrated, e.g., for $Nb_8W_9O_{47}$ [5] and Cr_2Hf [6].

In this contribution, we apply HAADF-STEM for the characterization of niobium tungsten oxides. Starting with the fully oxidized phase $Nb_8W_9O_{47}$, the formal substitution of two Nb^{5+} by Nb^{4+} and W^{6+} results in a solid solution series $Nb_{8-n}W_{9+n}O_{47}$ ($0 \leqslant n \leqslant 5$) with a constant ratio oxygen/metal but varying amounts of reduced cations as well as varying ratios Nb/W [7]. All these phases crystallize isostructurally in a threefold superstructure of the TTB type [8,9]. The TTB type was designated after K_xWO_3, which had been characterized by Magnéli already in 1949 [10]. The structure comprises a framework of corner-sharing octahedra that are stacked along the c-axis in such a way that tunnels with triangular, square and pentagonal shapes arise. The threefold TTB superstructure

*Corresponding author. Fax: +41 44 6321149.
E-mail address: krumeich@inorg.chem.ethz.ch (F. Krumeich).

0022-4596/$ - see front matter © 2006 Elsevier Inc. All rights reserved.
doi:10.1016/j.jssc.2006.02.020

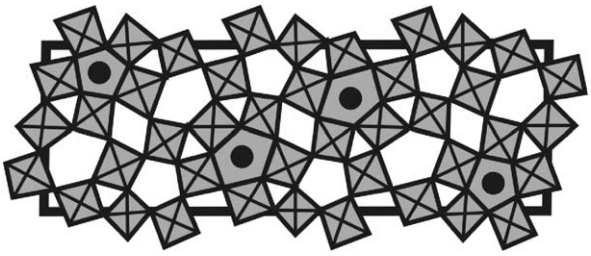

Fig. 1. Structural model of $Nb_8W_9O_{47}$ in projection onto the *ab* plane. A third of the pentagonal tunnels (PTs) is filled with metal–oxygen strings (represented by filled circles) in such a way that a threefold superstructure of the tetragonal tungsten bronze (TTB) type arises. The pentagons of octahedra around the filled PTs are connected via edge-sharing (so-called diamond link [19]).

of $Nb_8W_9O_{47}$ is formed by filling a third of the pentagonal tunnels with metal–oxygen strings systematically (Fig. 1). The oxidation of the reduced phases $Nb_{8-n}W_{9+n}O_{47}$ at high temperature ($T_{OX} = 1200\,^{\circ}C$) generally results in the formation of the thermodynamically stable phases whereas lower oxidation temperatures lead to products that contain several new structural elements and ordering varieties observed for the first time [11–13]. Here, we report on the results of a HAADF-STEM investigation of the oxidation products of $Nb_4W_{13}O_{47}$ obtained at $T_{OX} = 1000\,^{\circ}C$.

2. Experimental

2.1. Synthesis

$Nb_4W_{13}O_{47}$ (orthorhombic: $a = 1.225$, $b = 3.659$, $c = 0.3897$ nm) was prepared by heating a mixture of WO_3 and NbO_2 (molar ratio 13:4) in an evacuated silica vessel (1250 °C; 3d; mineralizer: $HgCl_2$), as described elsewhere [7]. The dark blue product was then ground and oxidized in air ($T_{OX} = 1000\,^{\circ}C$; 3d) [11].

2.2. Electron microscopy

Selected area electron diffraction (SAED) and STEM were performed on a *Tecnai 30F* transmission electron microscope (*FEI*; SuperTwin lens with $C_s = 1.2$ mm), operated at 300 kV (field emission gun, extraction voltage 4.4 kV). Crushed samples were suspended in ethanol and some droplets deposited on a holey carbon foil supported on a copper grid. The grid was mounted on a double tilt holder. In the diffraction mode, suitable thin crystal fragments were oriented along the short crystallographic axis to observe the crystal structure in projection on the *ab* plane. In the STEM mode of the TEM, a focused electron beam is scanned over a selected sample area. The resolution limit is determined by the smallest achievable spot size (about 0.2 nm). STEM images were recorded with a HAADF detector (image size: 1024×1024 pixels; scan times: 5–20 s; camera length: 200 mm), using almost exclusively incoherently scattered electrons (Rutherford scattering) for image formation resulting in atomic number (Z) contrast. An energy-dispersive X-ray (EDX) spectrometer (*EDAX*) attached to the *Tecnai F30* allows one to perform elemental analyses at spots selected in the HAADF-STEM images. Spot diameters in the range of 2–5 nm were applied for EDX analyses to achieve the required lateral resolution while giving a sufficiently high signal/noise ratio. For image processing, the program *Digital Micrograph* (*Gatan*) was used.

3. Results and discussion

$Nb_4W_{13}O_{47}$ is oxidized according to

$$Nb_4W_{13}O_{47} + O_2 = Nb_4W_{13}O_{49}.$$

The increased ratio oxygen/metal of $Nb_4W_{13}O_{49}$ ($O/\Sigma M = 2.882$) compared to that of $Nb_4W_{13}O_{47}$ ($O/\Sigma M = 2.765$) has to be compensated for by structural changes. At high oxidation temperatures ($T_{OX} = 1200\,^{\circ}C$), $Nb_4W_7O_{31}$ and WO_3 are formed according to

$$Nb_4W_{13}O_{49} = Nb_4W_7O_{31} + 6WO_3$$

as expected from the phase diagram [11,14]. In contrast to that, low oxidation temperatures ($T_{OX} \leqslant 1000\,^{\circ}C$) result in the formation of different, apparently metastable structural variants. At $T_{OX} = 1000\,^{\circ}C$, two different structure types occur in the oxidation product. Besides the basic reflections of the TTB substructure ($a = b \approx 1.22$ nm), the electron patterns of both types exhibit diffuse scattering indicating disorder. Type I is characterized by streaks along one or both $\langle 110 \rangle^*_{TTB}$ directions (Fig. 2a) [11]. Electron diffraction patterns of Type II show diffuse scattering in the shape of a cross, with maxima of intensity located close to $\{1/2,1/2,0\}^*_{TTB}$ and $\{3/2,1/2,0\}^*_{TTB}$ (Fig. 2b) [13]. HAADF-STEM images of both types will be presented and discussed in the following section.

3.1. Type I

A typical HAADF-STEM image of $Nb_4W_{13}O_{49}$ ($T_{OX} = 1000\,^{\circ}C$) shows planar defects occurring in two perpendicular orientations (Fig. 3a). Between these defects, an intact TTB structure is present, which contains Nb and W according to EDX spot analyses (Fig. 3b). In some of the planar defects, an almost square array of bright dots is visible. The high brightness of the dots in these ReO_3-type domains compared to those present in the adjacent bronze-type $(Nb,W)O_x$ matrix indicates a higher amount of W (Z contrast). EDX analyses performed at spots inside such domains indeed prove the presence of only W. The characteristic X-rays of W (strong peaks: L at ~8.4 and 9.7, M at ~1.8 keV) appear in both spectra (Fig. 3b and c), whereas those of Nb (strong peaks: K at ~16.5, L at ~2.3 keV) are present in that of the matrix only (Fig. 3c). Therefore, the oxygen excess of the oxidation product $Nb_4W_{13}O_{49}$ is partly compensated for by segregation

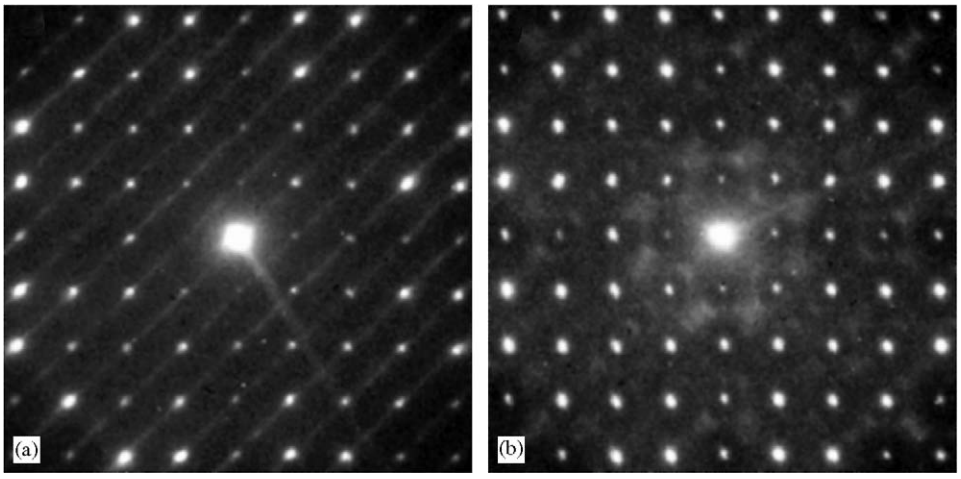

Fig. 2. Selected area electron diffraction (SAED) patterns (a^*b^* plane) of $Nb_4W_{13}O_{47}$ oxidized at 1000 °C; (a) type I: diffuse streaks along $[110]_{TTB}$, (b) type II: cross-shaped diffuse scattering.

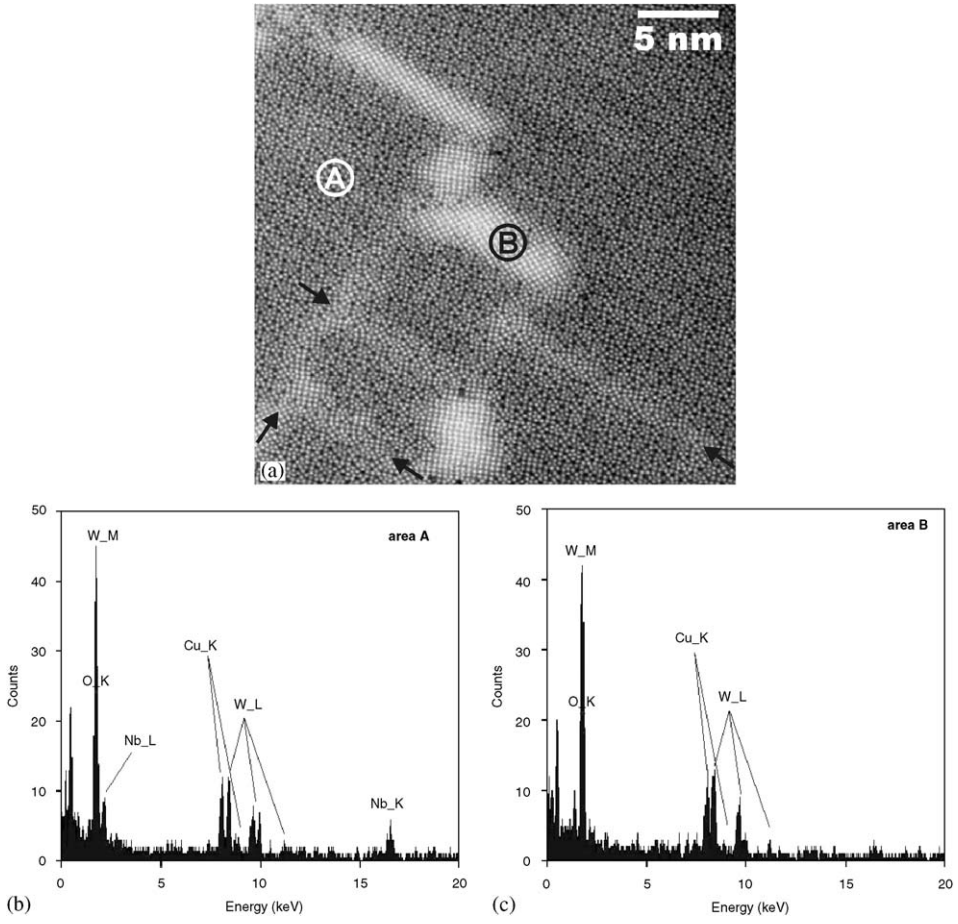

Fig. 3. (a) Processed high-angle annular dark field scanning transmission electron microscopy (HAADF-STEM) image of $Nb_4W_{13}O_{47}$ oxidized at 1000 °C (type I) showing segregations of WO_3 (square arrays of bright dots) and planar defects (arrows). (b), (c) EDX spectra of the areas encircled in (a); (b) area A and (c) area B. The X-rays with energies typical for Nb (K peaks at ~16.5, L at ~2.3 keV) appear only in the EDX spectrum of the matrix (area A).

of WO_3 like in the oxidation product obtained at $T_{OX} = 1200$ °C. The angles between lines of spots in these domains are supposed to be close to 90° since the almost square array of spots correspond to cuttings of the WO_3 structure. It should be noted that the occasional distortion of these angles is either due to instability during image recording like sample drift or to an inaccurate alignment of the microscope's STEM mode.

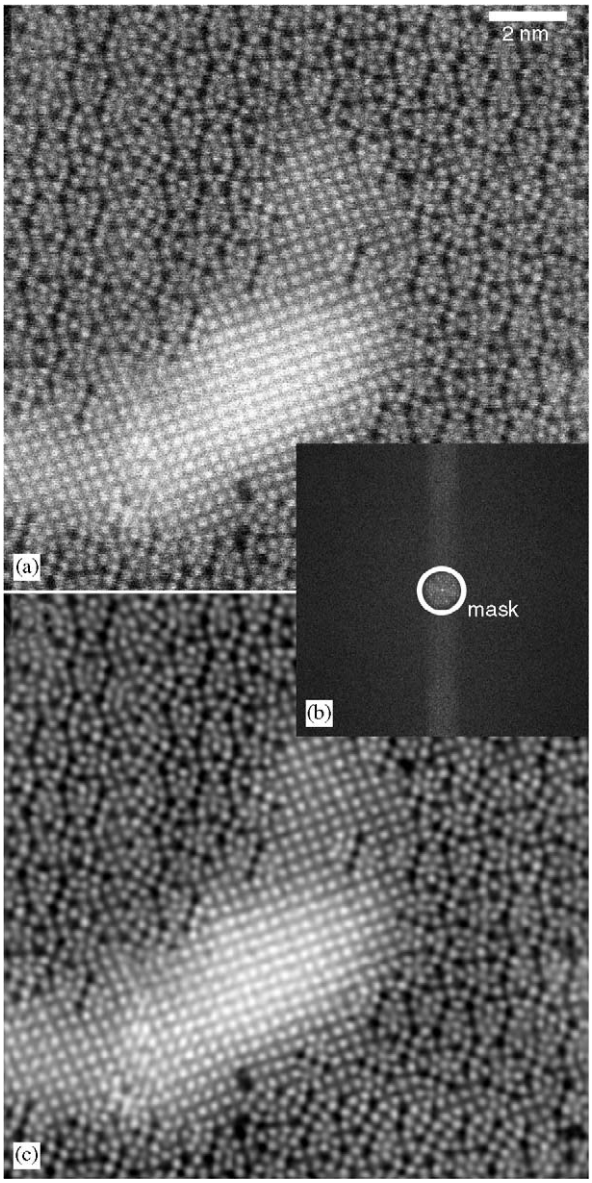

Fig. 4. $Nb_4W_{13}O_{47}$ oxidized at 1000 °C, type I. (a) Raw HAADF-STEM image. (b) Fast Fourier transform (FFT) of (a). Only the reflections inside the mask were used for the calculation of the inverse fast Fourier transform (IFFT, processed HAADF-STEM image, (c)).

A higher magnified area containing a WO_3 domain embedded into the TTB-type matrix is shown in Fig. 4. The original image obtained was compressed in vertical direction by about 16%. This distortion was corrected by elongating the image till the angles in the ReO_3-type segregations were adjusted to be about 90°. The image processing subsequently applied improves the image quality in the following way. Caused by instabilities during the scanning process, the bright patches corresponding to the metal positions are not perfect circles but show streaks in horizontal direction. The calculated diffraction pattern consequently exhibits side bands in vertical directions (Fig. 4b). To get rid of this, a mask is applied that allows only the reflections in the central disk to contribute to the inverse FFT (Fig. 4c). As a result, the unwanted signal decreasing image quality is removed, and the processed HAADF-STEM image looks much sharper, with the bright patches being more circular now. A similar but less pronounced improvement can be reached by applying the spatial filter *smooth* of the *Digital Micrograph* program (low pass filtering).

Besides the segregations of WO_3, planar defects occur that comprise uncommon edge-sharing double pentagons of $(Nb,W)O_6$ octahedra (Fig. 5). Along these defects, the

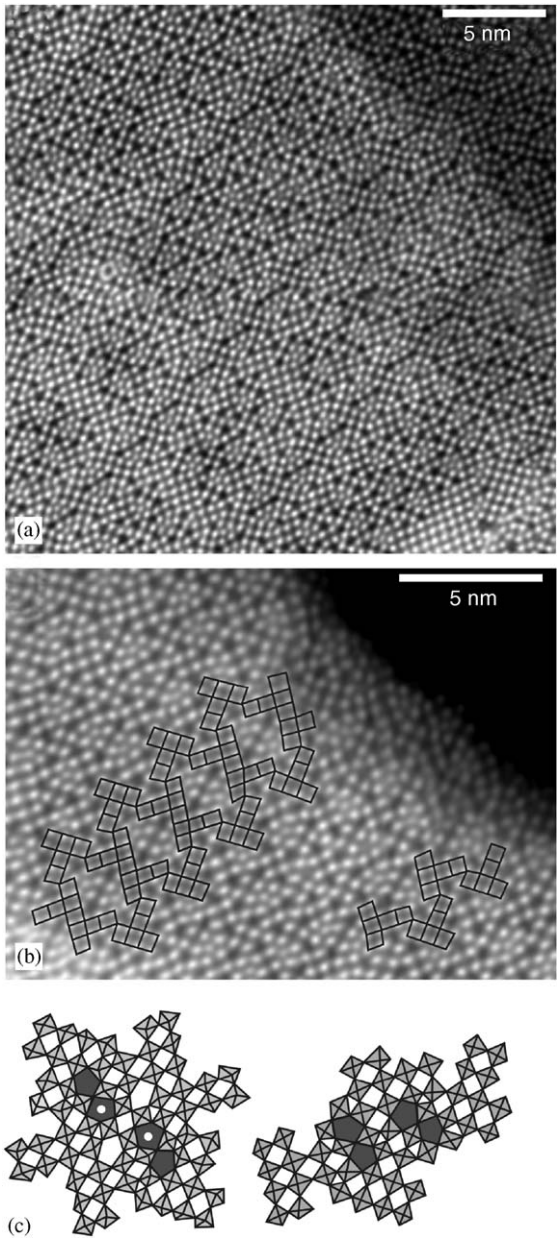

Fig. 5. $Nb_4W_{13}O_{47}$ oxidized at 1000 °C, type I. (a) Processed HAADF-STEM image of a large region. In (b) a simplified representation of the T-shaped arrays of octahedra is superimposed on the HAADF-STEM image. (c) Structural model of the octahedral arrangements in the defects. Double pentagons of octahedra are shaded gray.

structure is quasi-one-dimensionally periodic (Fig. 5a and b). The most common variant observed consists of alternating double pentagons and T-shaped arrays of squares of corner-sharing octahedra (Fig. 5b and c on the right side). Such planar defects, which have been discussed in detail elsewhere [11], as well as WO_3 domains are coherently embedded in the TTB-type matrix structure due to the close geometrical relationship between ReO_3 and the TTB type [15]. This is nicely demonstrated by another arrangement observed here for the first time. Two strings of the defects discussed above are fused together in such a way that the T-shaped octahedral arrays point in opposite directions and share a square of octahedra with each other (Fig. 5b and c on the left side). In the center of the fused T's, an intact TTB subcell is incorporated. In general, the incorporation of these planar defects and the WO_3 domains into the TTB-type matrix occurs parallel to $\langle 110 \rangle_{TTB}$ in a disordered way which leads to the diffuse streaks observed in the SAED pattern (Fig. 2a).

3.2. Type II

An HAADF-STEM image of a crystal which gives rise to a SAED pattern of type II (Fig. 2b) is shown in Fig. 6. The TTB substructure is almost free of defects. Only few units of 4×4 bright patches can be detected which represent arrays of 4×4 WO_6 octahedra. In connection with the surrounding TTB-type structure, these arrays correspond to isolated unit cells of $Nb_4W_7O_{31}$ [15,16]. The incorporation of this relatively O-rich phase ($O/\Sigma M = 2.818$) apparently accommodates a part of the O excess in $Nb_4W_{13}O_{49}$ ($T_{OX} = 1000\,^{\circ}C$) [13].

The FFT of the HAADF-STEM image (inset in Fig. 6) shows diffuse scattering with the shape of a cross as it is present in the corresponding SAED pattern as well (Fig. 2b). Since only the cation positions are visible in the high-resolution STEM images, the observed short-range order is clearly caused by their arrangement. It is well-known that in Nb–W oxides this phenomenon generally concerns the occupancy of the pentagonal tunnels (PT) with metal–oxygen strings [17,18]. Rather than filling the PT randomly, only a part of them contains metal in a rather systematic way (Fig. 7). Typically, long slabs of filled PTs connected via a square of octahedra (diamond link

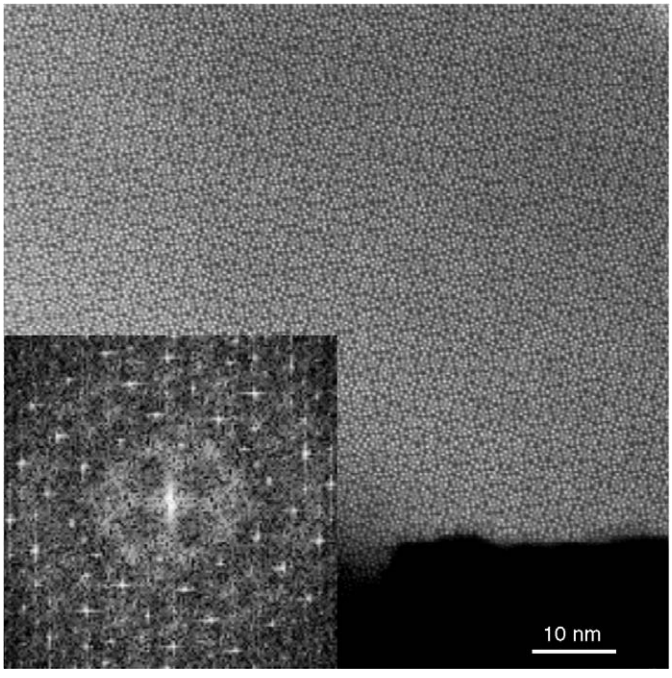

Fig. 6. $Nb_4W_{13}O_{47}$ oxidized at 1000 °C, type II. Processed HAADF-STEM image. The FFT pattern (inset) shows diffuse scattering in the shape of a cross besides the reflections of the basic TTB structure.

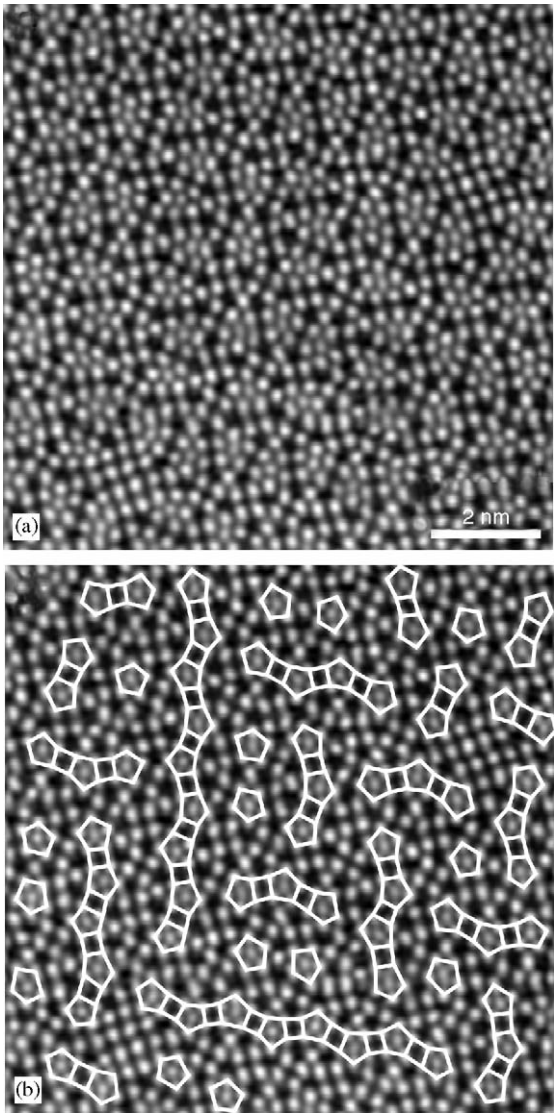

Fig. 7. $Nb_4W_{13}O_{47}$ oxidized at 1000 °C, type II. (a) Processed HAADF-STEM image. In (b) a simplified representation, which shows the cation positions of pentagonal tunnels filled with metal–oxygen strings connected by lines, is superimposed on the HAADF-STEM image. Two arrays of 4×4 WO_6 octahedra (4×4 bright dots) are present (upper right and lower left side).

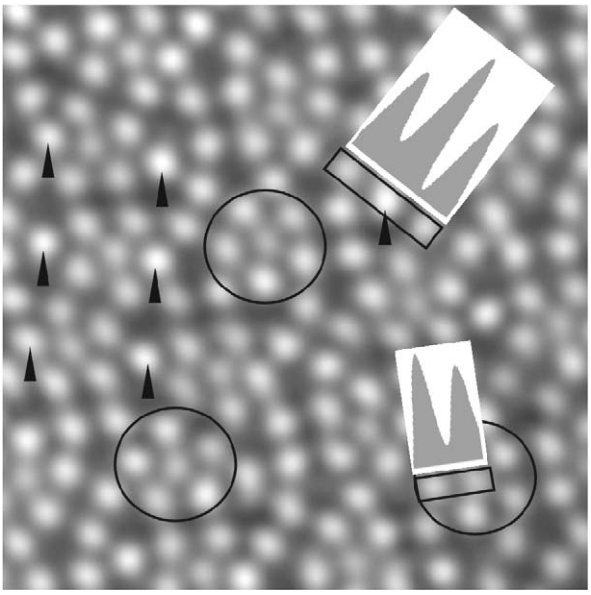

Fig. 8. Processed HAADF-STEM image of $Nb_4W_{13}O_{47}$ ($T_{OX} = 1000\,^{\circ}C$), type II. Intensity profiles insets show that the metal positions in the center of two triangular and two pentagonal tunnels (some marked by arrows) have the highest brightness whereas such occupying pentagonal tunnels (encircled) appear relatively dark.

[19], cf. Fig. 1) occur running along two perpendicular $\langle 110 \rangle^*_{TTB}$ directions (Fig. 7b). The underlying structural principle was comprehensively discussed before [13]. Since less PTs are filled in this structure ($(MO)_x(M_{10}O_{30})$ with $x \approx 7/6$ [13]) than in the starting phase ($Nb_4W_{13}O_{47} \equiv (MO)_{4/3}(M_{10}O_{30})$), this disordered oxidized structure contains more oxygen.

The brightness of the metal positions varies quite widely, and a systematic arrangement of the brightest patches is not recognizable on the first view (Fig. 7a). Remarkably, at two positions, a clear, systematic tendency for the metal occupancy is observed (Fig. 8). All positions inside the PTs appear darker than the surrounding ones indicating a lower scattering potential there. Thus, the amount of the weak scatterer Nb (low atomic number Z compared to W with a much higher Z) is high there (Fig. 8). This is in accordance with the results of X-ray diffraction investigations on single crystals of $Nb_8W_9O_{47}$ [8] and of $Nb_7W_{10}O_{47}$ [9] that both have detected a high occupancy of this position by Nb (about 0.84). However, a partial occupancy of the PTs by W would lead to a similarly weak signal at this position. In spite of the lack of experimental evidence, this cannot be excluded completely. It has to be stated that the same intensity distribution is recognizable in the unprocessed as well as in the processed HAADF-STEM images. Furthermore, a related HAADF-STEM study of $Nb_8W_9O_{47}$ [5] revealed the occupancy of symmetry-related positions by W and Nb rather accurately. Compared to that phase with a metal ratio W/Nb = 9:8, the sample investigated in this study has a much higher W content (W/Nb = 13:4). Therefore, the intensity variation between differently occupied positions is expected to be smaller in $Nb_4W_{13}O_{47}$. Remarkably, the positions in the center of two triangular and two pentagonal tunnels always appear with very high brightness (Fig. 8). This position was indeed found to be exclusively occupied by W in $Nb_8W_9O_{47}$ [8] and $Nb_7W_{10}O_{47}$ [9]. The preference of W for this position is apparently preserved in this less-ordered TTB structure. This observation furthermore indicates that the site occupancy in the starting compound $Nb_4W_{13}O_{47}$ as determined by symmetry relation between crystallographic equivalent positions is not completely lost during the oxidation process in spite of the necessary migration of metal atoms during the structural rearrangement.

4. Conclusions

The experimental results presented here demonstrate that HAADF-STEM imaging is a valuable technique for the investigation of ReO_3- and bronze-type structures. As in HRTEM images of niobium tungsten oxides utilizing phase contrast, it is possible to discern the positions of the metal atoms in the centers of oxygen polyhedra in HAADF-STEM images recorded along the short crystallographic axis and to derive structural models from that projection. Since HAADF-STEM imaging almost only uses electrons scattered incoherently into high angles and thus signals depend strongly on the atomic number of the scattering atom (Z contrast), additional chemical information can be obtained. Furthermore, EDX analyses at selected spots with diameters in the nm size range can easily be accomplished. Compared to HRTEM, however, HAADF-STEM is the more demanding imaging technique from a practical point of view. Because image recording is serial, measuring the signal point-wise, this imaging technique requires rather long exposure time (here: 5–20 s; cf. 0.5–2 s for HRTEM) so that even a small sample drift has a deteriorating effect on image quality. Furthermore, image distortions because of magnetic stray fields, vibrations, or misalignments of the microscope's STEM mode might occur that can only be corrected partly. Inaccuracies of the crystal orientation and a not optimally adjusted electron beam have even more serious effects on image quality than in HRTEM. The image contrast can be considerably reduced by contamination with a carboneous layer formed by cracking residual hydrocarbons in the intense electron beam. Consequently, image processing is more important in high-resolution STEM than in HRTEM to obtain optimized images. HAADF-STEM (or Z contrast) imaging represents an important alternative technique for structure determination by electron microscopy means since directly interpretable structural images simultaneously provide supplementary information about elemental distribution at atomic resolution.

References

[1] S. Iijima, J. Allpress, Acta Crystallogr. A 30 (1974) 22–29.
[2] S.J. Pennycook, Ultramicroscopy 30 (1989) 58–69.
[3] R.F. Klie, Y. Zhu, Micron 36 (2005) 219–231.
[4] M. Varela, A.R. Lupini, K. van Benthem, A.Y. Borisevich, M.F. Chisholm, N. Shibata, E. Abe, S.J. Pennycook, Annu. Rev. Mater. Res. 35 (2005) 539–569.
[5] A.I. Kirkland, W.O. Saxton, J. Microsc. 206 (2002) 1–6.
[6] M.F. Chisholm, S. Kumar, P. Hazzledine, Science 307 (2005) 701–703.
[7] F. Krumeich, A. Hussain, C. Bartsch, R. Gruehn, Z. Anorg. Allg. Chem. 621 (1995) 799–806.
[8] A.W. Sleight, Acta Chem. Scand. 20 (1966) 1102–1112.
[9] F. Krumeich, M. Wörle, A. Hussain, J. Solid State Chem. 149 (2000) 428–433.
[10] A. Magnéli, Ark. Kemi 1 (1949) 213–221.
[11] F. Krumeich, C. Bartsch, R. Gruehn, J. Solid State Chem. 120 (1995) 268–274.
[12] F. Krumeich, J. Solid State Chem. 119 (1995) 420–427.
[13] F. Krumeich, Acta. Crystallogr. B 54 (1998) 240–249.
[14] M.W. Viccary, R.J.D. Tilley, J. Solid State Chem. 104 (1993) 131–148.
[15] B.G. Hyde, M. O'Keeffe, Acta. Crystallogr. A 29 (1973) 243–248.
[16] R.S. Roth, J.L. Waring, J. Res. Natl. Bur. Stand. A 70 (1966) 281–303.
[17] R. De Ridder, G. Van Tendeloo, D. Van Dyck, S. Amelinckx, Phys. Stat. Sol. A 41 (1977) 555–560.
[18] S. Horiuchi, K. Muramatsu, Y. Matsui, J. Appl. Crystallogr. 13 (1980) 141–147.
[19] M. Lundberg, M. Sundberg, A. Magnéli, J. Solid State Chem. 44 (1982) 32–40.